

J.T. ZENG[✉]
K.Y. ZHAO
H.R. ZENG
H.Z. SONG
L.Y. ZHENG
G.R. LI
Q.R. YIN

Subsurface defect of amorphous carbon film imaged by near field acoustic microscopy

The State Key Laboratory of High Performance Ceramics and Superfine Microstructure, Shanghai Institute of Ceramics, Chinese Academy of Sciences, Shanghai 200050, P.R. China

Received: 17 September 2007/Accepted: 7 January 2008
Published online: 14 February 2008 • © Springer-Verlag 2008

ABSTRACT Amorphous carbon films were examined by low frequency scanning-probe acoustic microscopy (LF-SPAM). Local elastic properties as well as topography were imaged in the acoustic mode. Two kinds of subsurface defects were revealed by the LF-SPAM method. The influence of the subsurface defects on the elastic properties was also discussed. The ability to image subsurface defects was dependent on the scan area and the scan speed. Our results showed that the low frequency scanning-probe acoustic microscopy is a useful method for imaging subsurface defects with high resolution.

PACS 68.37.Ps; 68.37.Uv; 61.43.Dq; 68.35.Gy

1 Introduction

Amorphous carbon films have received considerable attention recently due to their interesting diamond-like properties [1–3]. Amorphous carbon prepared by various methods can have any mixture of sp^3 , sp^2 , or sometimes sp sites. It can have a high elastic hardness, chemical inertness, and optical transparency. Thus, these films have potential applications as protective coatings in areas such as optical windows, magnetic storage disks, car parts, biomedical coatings, and as micro-electromechanical devices (MEMS).

There are many references which report the elastic properties of amorphous carbon films, such as adhesion, wear resistance, hardness, elastic modulus, and the Poisson ratio at a macro scale [4–8]. Some researchers have studied the elastic properties of amorphous films on the submicron scale by atomic force acoustic microscopy [9]. Most of the studies focused on the influence of composition and processing on the properties of amorphous carbon films. Besides those factors, subsurface defects should also play an important role in the mechanical properties of amorphous carbon films. A subsurface defect is invisible to optical and electronic microscopy, but it is not the case for an acoustic imaging method such as scanning acoustic microscopy (SAM). Unfortunately the resolution of an ordinary SAM is limited by the wavelength and is usually above the micron scale [10]. Acoustic imag-

ing method based on scanning-probe microscopy such as scanning microdeformation microscopy was shown to have the ability to produce subsurface images in both transmission and reflection modes, but the reported resolution was not very high ($> 10 \mu\text{m}$) which may be due to the large tip size (about $15 \mu\text{m}$) [11, 12]. There are also other dynamic force microscopy methods such as intermittent-contact AFM (IC AFM) [13], and ultrasonic force microscopy (UFM) [14]. The IC AFM is useful for imaging soft materials, but it is difficult to extract material properties. The IC AFM equipped with a torsional harmonic cantilever has the ability to allow elastic measurement [15], but the cantilever needs special treatment with the tip offset from the center of the cantilever. UFM can also be used to measure the elastic properties of materials, especially for stiff materials, but the tip is cyclically indented into the sample and the indentation should reach a threshold in order to be sensitive to the nonlinearity of the force-indentation curve. The UFM test should also be carried out with high vibrating frequency ($> 2 \text{ MHz}$). Scanning near-field ultrasound holography (SNFUH) has recently been successfully developed by Shekhawat et al. and it was used to observe the subsurface image of red cells and buried Au nanoparticles with high resolution (20 nm) [16], but the experimental setup is complicate and the working frequency is also high ($> 2 \text{ MHz}$). Because this kind of examination is usually based on a lock-in technique, the high working frequency is a challenge to the lock-in amplifier.

Low frequency scanning-probe acoustic microscopy (LF-SPAM) was successfully developed in our laboratory. Different from ordinary atomic force acoustic microscopy (AFAM) methods, the LF-SPAM method uses the excitation frequency below 30 kHz which is far below the contact resonance frequency which is used in the AFAM method (usually several hundred kHz). Furthermore, the static force applied at the tip in LF-SPAM is below 10 nN which is much smaller than in the ordinary AFAM method (above 50 nN). The low static force may be helpful to reduce damage of the sample. Our previous results showed that this method is very useful in domain characterization of ferroelectric crystals and ceramics [17, 18]. This method has never been used to examine amorphous material and whether it can image subsurface defects is still unknown. In this paper, we show some new features of low frequency near field acoustic microscopy characterization of amorphous carbon film and demonstrate the ability of the low

✉ Fax: +86-21-52413122, E-mail: zjt@mail.sic.ac.cn

frequency near field acoustic microscopy to image the subsurface defects of the material.

2 Experimental

Amorphous carbon films were grown on a polished Si substrate by the PVD method. The thickness of the film is about 100 nm. An atomic force microscopy in the acoustic mode was built by us based on a commercial atomic force microscope (AFM) (SPA 400, SPI3800N, Seiko Japan). A piezoelectric transducer is placed below and in contact with the sample. A 2 μm thick, 90 μm long Ti/Pt-coated Si cantilever (Micro Masch, NSC12-B) with a spring constant of 14 N/m and a resonance frequency of 315 kHz was used. The static force applied on the tip was set to 7 nN. An external function generator (33120 A, Agilent) provides sinusoidal excitation signals applied to the piezoelectric transducer, which gives rise to flexural vibration and emits acoustic waves into the sample and causes an out-of-plane and in-plane surface displacement. By setting the cantilever in contact with the sample surface, we can acquire the so-called acoustic images, which represent the vibration amplitude of the cantilever. The cantilever deflection from the out-of-plane component of surface displacement was measured through a lock-in amplifier (Model 7280 DSP, Signal Recovery Instrumentation). The acoustic images of every sample were acquired simultaneously with the topographical ones.

3 Results and discussion

Figure 1a shows the topography image of an amorphous carbon film with a scan area of 2 $\mu\text{m} \times 2 \mu\text{m}$. The surface of the film is quite smooth and the mean surface roughness (RMS) is about 0.1015 nm. The bright areas in the image indicate high altitude and dark areas indicate low altitude. The acoustic image (Fig. 1b) is very different from the topography image. It is quite uniform in the scan area and shows few features of the topography. From this point, the SPAM characterization of amorphous carbon film is differ-

ent from that of the ceramics samples. When characterizing the ceramics samples, the acoustic image usually matches well with the topography image and the acoustic image has a much higher resolution than the topography image [19]. It is reasonable when considering the imaging mechanism of SPAM which is based on the variation of local elastic properties [20, 21]. Grains in the polycrystalline ceramics have different crystal orientation with different elastic properties, thus the acoustic image is much clearer than the topography image. For amorphous carbon film the elastic properties are isotropic, so the acoustic image is quite uniform and reveals few topography features.

Figure 2 shows the topography images and acoustic images at different frequencies, of another area. No important information can be found in the topography image, but there is a bright region marked as “A” in the acoustic image, and a dark region marked as “B” within the bright region (Fig. 2b). The contrast of region A changes from bright to dark on decreasing the test frequency from 10.3 kHz to 6 kHz, but the contrast of region B stays dark, so the whole region shows dark contrast. On increasing the test frequency from 10.3 kHz to 14 kHz, the contrast of region B changes from dark to bright, but the contrast of region A remains bright, so the whole region shows bright contrast. Contrast reversal can also be observed in other high frequency AFAM methods when acquiring the acoustic image below or above the contact resonance frequency [21]. Because the acoustic image reveals the variation of local elastic properties, these areas should have different elastic properties from other parts. The regions A and B should indicate different types of defects because they have different contrast reversal frequencies. In order to know the exact nature of the defects, the area was scanned ten times. It is found that the topography changes gradually during the scanning process. Figure 2e shows the topography after scanning ten times. It can be seen that the profile of the defect appeared in the topography image. Since the topography image only indicates the altitude of the film, the film in the defect region should have been detached from the substrate. It is quite clear that the defect in region A is a void between the

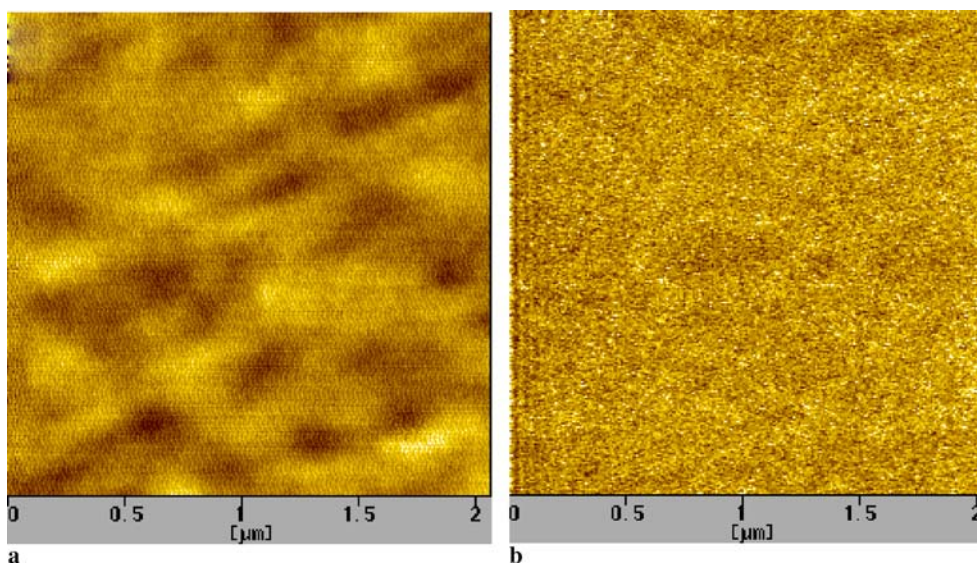


FIGURE 1 The topographic image (a) and acoustic image (b) of an amorphous carbon film

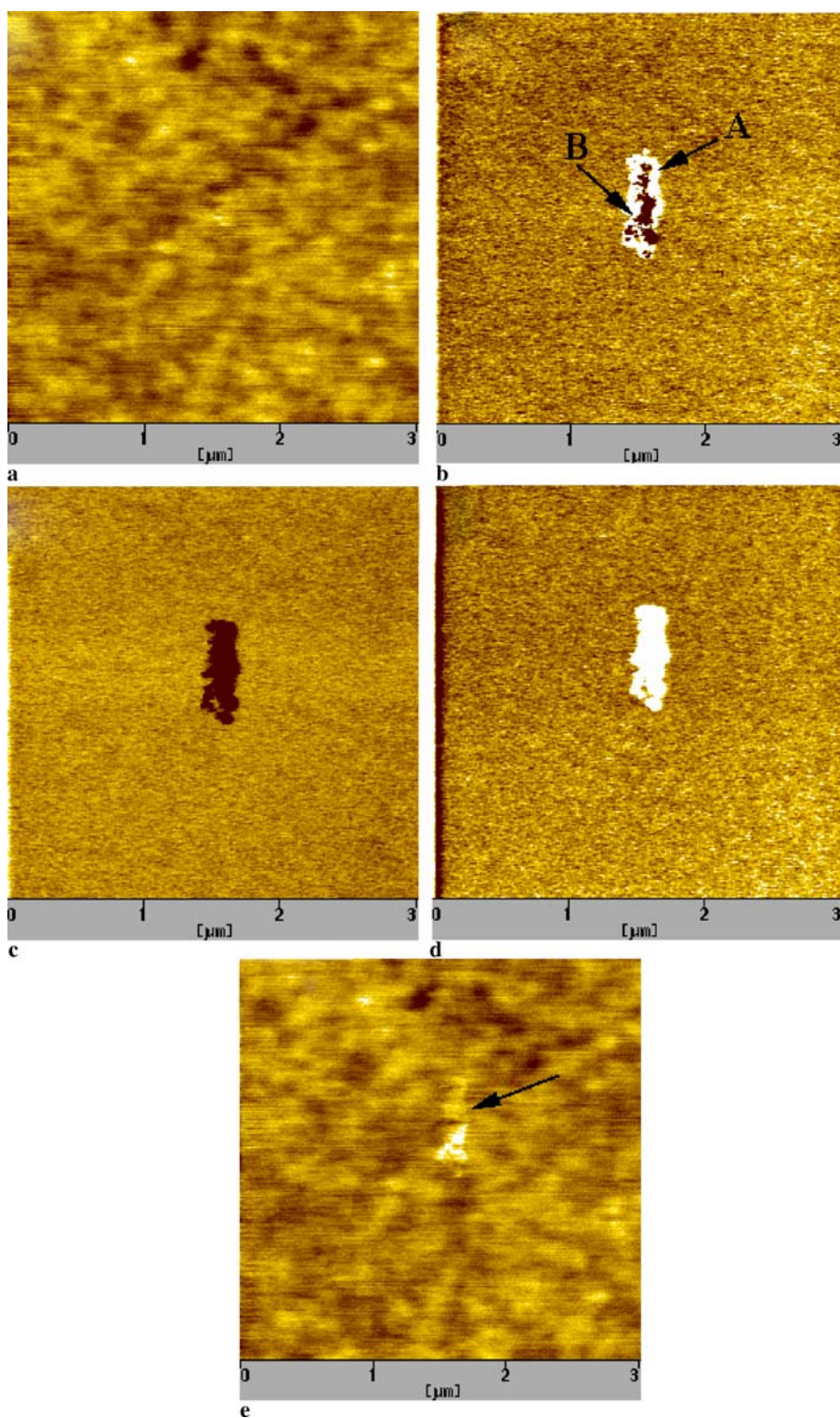


FIGURE 2 (a) The topographic image and acoustic image of amorphous carbon film at different frequencies: (b) 10.3 kHz; (c) 14 kHz; (d) 6 kHz; (e) the topography image of amorphous carbon film scanned ten times

film and the substrate. The film is smooth at first and detached from the substrate by the scratch of the tip.

Figure 3 shows the enlarged topography image and acoustic image of Fig. 2. Even after the film in region A detached from the Si substrate, and it is visible in the topography image (Fig. 3a), region B is still invisible in the topography image, but it can be clearly seen in the acoustic image (Fig. 3b). The defect in region B may be caused by the secondary phase or

contamination on the bottom of the film. From the acoustic image, we can also notice there are some points in region A have the same contrast with the defect-free region which indicate that they still stick to the substrate. The width of the point is about 10 nm obtained from the line scan, which means that this method can achieve very high resolution. Cretn studied the observation depth in scanning microdeformation microscopy and found that the investigation depth was about

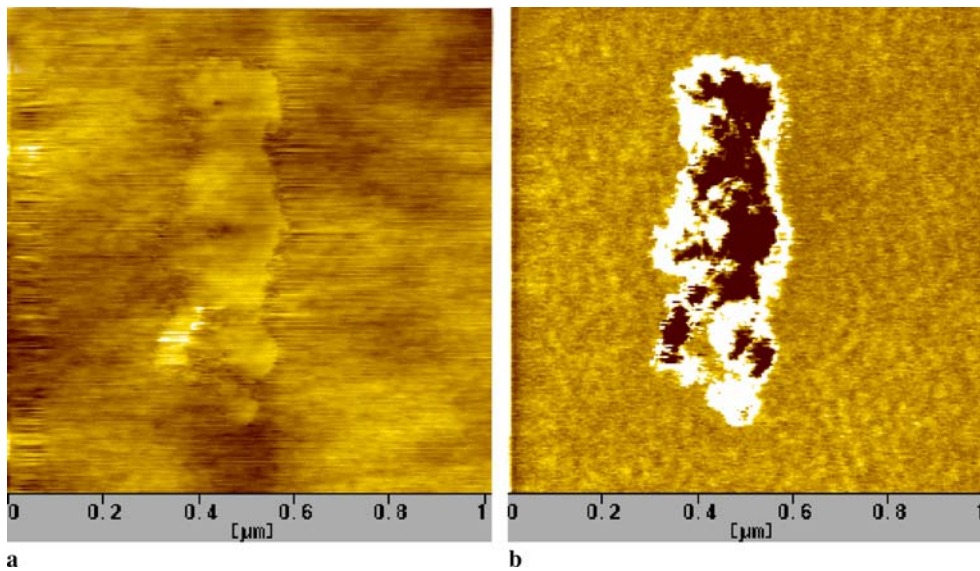


FIGURE 3 Enlarged topographic image (a) and acoustic image at 10.3 kHz (b) of Fig. 2

50 times that of the contact surface [22]. In this work, the defects were 100 nm below the surface and the radius of the tip is about 10 nm. The defects were within the depth range of changes of contact stiffness.

In the AFAM system, the contrast reversal results from different amplitudes below and above the contact resonance frequency, and the resonance frequency is strongly related to the elastic properties of the material being tested. The contrast reversal in this work should have a similar mechanism. From Figs. 2 and 3, the scanned amorphous carbon can be divided into 3 parts: defect free region C (apart from region A and region B), delaminated region (A), delaminated and contaminated region (B). These three regions have different resonance frequencies, denoted as $f_{res,C}$, $f_{res,A}$ and $f_{res,B}$ ($f_{res,B} < f_{res,A} < f_{res,C}$) respectively. The vibration amplitude of the tip versus frequency at the three regions is shown schematically in Fig. 4. It can be seen that the test frequency 14 kHz is located above $f_{res,C}$, thus the amplitude of region A and B is lower than that of the defect free region, and both region A and B show a dark color. The test frequency 10.3 kHz is located between $f_{res,B}$ and $f_{res,A}$, thus the amplitude of the

defect free region is larger than that of region B but lower than that of region A, so region B shows dark color but region A shows a bright color. The test frequency 6 kHz is located below $f_{res,B}$, thus the amplitude of the defect free region is lower than that of region A and B, so both region A and B show bright color. The frequency shift due to the change of elastic properties was also observed by Crozier et al. and they found that with the increase of the thickness, the resonance frequency of stiff film increased and the resonance frequency of soft film decreased [23].

The resonance frequency of the film is also related to the elastic properties [24]. From the Heterzan Mode, the elastic constant can be calculated by:

$$k^* = \sqrt[3]{6E^*RF_c}, \quad (1)$$

where R is the radius of curvature of the tip. F_c is the static force applied on the tip and E^* is the effective elastic constant of the tip-sample contact region and can be expressed as

$$\frac{1}{E^*} = \frac{1 - \nu_t}{E_t} + \frac{1 - \nu_s}{E_s}, \quad (2)$$

where E_t , ν_t , E_s and ν_s are Young's modulus and Poisson's ratio of the tip and the sample surface, respectively. The ratio of the elastic constants of the two regions can be expressed as

$$\frac{E_1^*}{E_2^*} = \left[\frac{k_1^*}{k_2^*} \right]^{3/2}, \quad (3)$$

the elastic constant can be calculated from the following

$$f_{res} = \sqrt{\frac{k^* + k_c}{m}}, \quad (4)$$

where k_c is the spring constant of the cantilever and m is the mass of the tip when considering it by a point mass model. From the above formula, we can see that delamination of the film will reduce the elastic module and the elastic module will be further reduced by the contamination below the film. The reduction of the elastic module caused by the defects will certainly deteriorate the performance of the film.

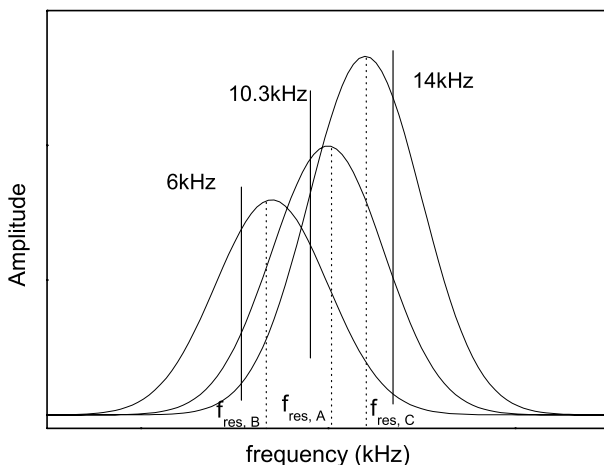


FIGURE 4 Schematic of the oscillation amplitude of the cantilever as a function of exciting frequency

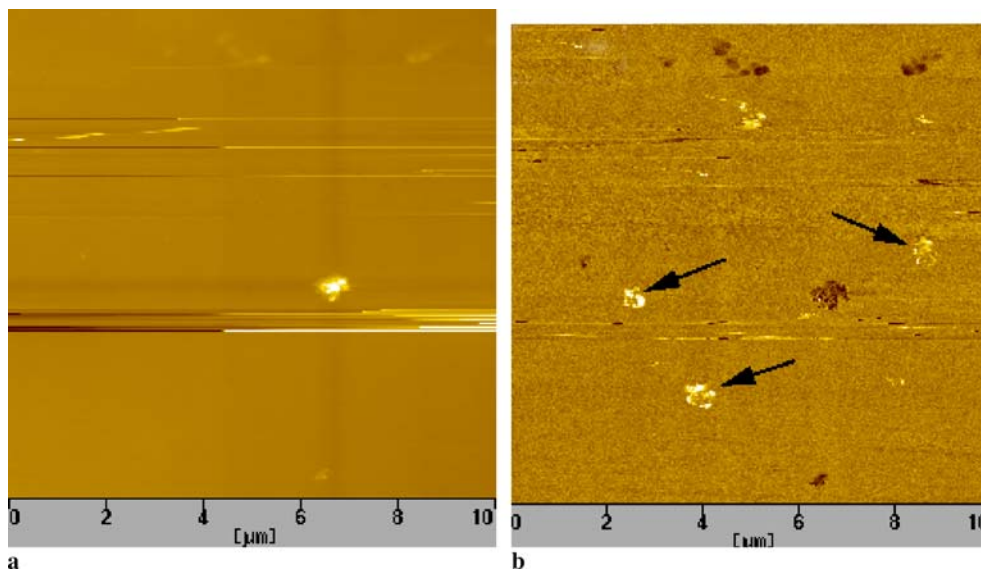


FIGURE 5 The topography image (a) and acoustic image (b) of amorphous carbon film with a scan area of $10\ \mu\text{m} \times 10\ \mu\text{m}$ and a scan speed of 0.08 Hz

It should also be noted that the resonance frequency is only several kHz which is far below the free resonance of the tip (315 kHz). It is different from the ordinary AFAM method in which the tip should have contact resonance frequency much higher than its free resonance frequency. The resonance behavior results from the vibration of the coupled system other than the tip.

These types of defects can be seen in some areas of the film. Whether they can be detected is strongly dependent on the size of the scan area. It can be detected easily in the acoustic image with the scan area $3\ \mu\text{m} \times 3\ \mu\text{m}$, but it is never found in the acoustic image with the scan area $10\ \mu\text{m} \times 10\ \mu\text{m}$ at the same scan speed (0.83 Hz). If we lower the scan speed, the defect can also be detected in the large scan areas. Figure 5 shows the topography and the acoustic image with the scan area $10\ \mu\text{m} \times 10\ \mu\text{m}$ and scan speed 0.08 Hz (Fig. 5a). It can be seen that there are two defect areas which can be found in the acoustic image by comparing the two images. It indicates that decreasing the scan area or scan speed is beneficial to the elastic mapping of amorphous carbon films. The results agree with that observed in the UFM test by Dinelli et al. [25]. They found that in order to perform UFM mapping, the amplitude modulation frequency must be high enough (compared to the scan speed) to perform at least one cycle over each single point of acquisition.

4 Conclusion

In summary, amorphous carbon film was examined by low frequency scanning-probe acoustic microscopy. The results showed that local elastic properties rather than the topography were imaged in acoustic mode. Two kinds of subsurface defects were shown by the SPAM method. Decreasing the scan area or scan speed is helpful in detecting a defect. It was demonstrated that the low frequency scanning probe acoustic microscopy is a useful method for mapping subsurface defects.

ACKNOWLEDGEMENTS This work was supported by the National Advanced Materials Committee of China (863-project No. 2007AA03Z330), the Natural Science Foundation of China (0774113) and the Innovation Project of the Shanghai Institute of Ceramics (SCX-0612).

REFERENCES

- 1 J. Robertson, *Mater. Sci. Eng. R* **37**, 129 (2002)
- 2 F.W. Smith, *J. Appl. Phys.* **55**, 764 (1984)
- 3 B.S. Satyanarayana, A. Hart, W.I. Milne, J. Robertson, *Appl. Phys. Lett.* **71**, 1430 (1997)
- 4 Q. Wei, R.J. Narayan, A.K. Sharma, J. Sankar, J. Narayan, *J. Vac. Sci. Technol. A* **17**, 3406 (1999)
- 5 N. Savvides, T.J. Bell, *J. Appl. Phys.* **72**, 2791 (1992)
- 6 S.J. Cho, K.R. Lee, J.H. Eun, K.Y. Jeong, D. Kwon, *Diam. Relat. Mater.* **8**, 1067 (1999)
- 7 D. Schneider, M.D. Tucker, *Thin Solid Films* **290**, 305 (1996)
- 8 H.L. Chan, U. Ekanayake, A. Kumar, M.R. Alam, Q. You, R.B. Inturi, N. Shu, J.A. Barnard, *Appl. Surf. Sci.* **109**, 58 (1997)
- 9 D. Passeri, A. Bettucci, M. Germano, M. Rossi, A. Alippi, *Appl. Phys. Lett.* **88**, 121910 (2006)
- 10 Z. Yu, S. Boseck, *Rev. Mod. Phys.* **67**, 863 (1995)
- 11 B. Cretin, F. Sthali, *Appl. Phys. Lett.* **62**, 829 (1993)
- 12 P. Vairac, B. Cretin, *Appl. Phys. Lett.* **68**, 461 (1996)
- 13 N.A. Burnham, O.P. Behrend, F. Oulevey, *Nanotechnology* **8**, 67 (1997)
- 14 F. Dinelli, S.K. Biswas, G.A.D. Briggs, O.V. Kolosov, *Phys. Rev. B* **61**, 13995 (2000)
- 15 O. Sahin, S. Magonov, C. Su, C.F. Quate, O. Solgaard, *Nature Nanotechnol.* **2**, 507 (2007)
- 16 G.S. Shekhawat, V.P. Dravid, *Science* **310**, 89 (2005)
- 17 H.R. Zeng, H.F. Yu, S.X. Hui, R.Q. Chu, G.R. Li, H.S. Luo, Q.R. Yin, *Solid State Commun.* **133**, 521 (2005)
- 18 H.F. Yu, H.R. Zeng, X.D. Ma, R.Q. Chu, G.R. Li, H.S. Luo, Q.R. Yin, *Phys. Stat. Solidi A* **202**, R10 (2005)
- 19 H.R. Zeng, H.F. Yu, L.N. Zhang, R.Q. Chu, G.R. Li, Q.R. Yin, *Phys. Stat. Solidi A* **202**, R41 (2005)
- 20 U. Rabe, S. Amelio, M. Kopycinska, S. Hirsekorn, M. Kempf, M. Göken, W. Arnold, *Surf. Interf. Anal.* **33**, 65 (2002)
- 21 U. Rabe, M. Kopycinska, S. Hirsekorn, J. Muñoz Saldaña, G.A. Schneider, W. Arnold, *J. Phys. D Appl. Phys.* **35**, 2621 (2005)
- 22 L. Robert, B. Cretin, *Surf. Interf. Anal.* **27**, 568 (1999)
- 23 K.B. Crozier, G.G. Yaralioglu, F.L. Degertekin, J.D. Adams, S.C. Minne, C.F. Quate, *Appl. Phys. Lett.* **76**, 1950 (2000)
- 24 S. Banerjee, N. Gayathri, S.R. Shannigrahi, S. Dash, A.K. Tyagi, B. Raj, *J. Phys. D Appl. Phys.* **40**, 2539 (2007)
- 25 F. Dinelli, H.E. Assender, N. Takeda, G.A.D. Briggs, O.V. Kolosov, *Surf. Interf. Anal.* **27**, 562 (1999)